

Data Bit Assisted Adaptive IMM Filter for Carrier Phase Tracking Through Interference

Wengxiang Zhao
MMAE Department
Illinois Institute of Technology
Chicago, United States
wzhao42@hawk.iit.edu

Boris Pervan
MMAE Department
Illinois Institute of Technology
Chicago, United States
pervan@iit.edu

Abstract—In this paper, we develop a carrier phase estimation algorithm to allow GPS receivers to maintain continuous signal tracking through wideband radio frequency interference events. Due to the nature of the GPS signal, carrier phase estimation is a hybrid estimation problem, requiring simultaneous estimation of the discrete-time navigation data bits and the continuous carrier phase. We use an interacting multiple model algorithm with two measurement models corresponding to the two possible choices of navigation data bits (+1 and -1) over each 20 ms coherent integration interval. At the end of each interval, we extract the final state vector estimate by combining the two modes' estimation results using their likelihood functions. We present experimental results to evaluate the performance of the IMM filter during wideband interference events.

Index Terms—GPS receiver, Wideband Interference, Carrier Phase Tracking, Interacting Multiple Model

I. INTRODUCTION

In this work, we develop a carrier phase estimation algorithm for GPS receivers that are subjected to wideband radio frequency interference (RFI). This technique allows receiver to effectively track continuous carrier phase and estimate discrete navigation data bits simultaneously. The concept is directly applicable to stationary GPS reference receivers and, when inertial aiding is available, moving receivers as well.

The example application we consider to evaluate performance is a Ground-Based Augmentation System (GBAS) reference station receiver subjected to broadband interference — for example, from nearby use of personal privacy devices (PPDs). Prior work has shown that PPDs most commonly emit broadband interference, and GBAS ground based reference receivers have experienced tracking discontinuities as a result [1]. These events can cause navigation service interruptions to aircraft on final approach. To ensure continuity of the navigation service GBAS reference stations must be able to track GPS signals in the presence of wideband interference.

During an RFI event, as long as existing satellites can be continuously tracked, it is not necessary to acquire new satellites or decode GPS navigation data bits. The reason is that GPS interface specifications ensure that there will always be at least a two-hour overlap of the intervals of applicability between two successive ephemerides broadcast by any satellite. This means that any ephemeris decoded just prior to the onset of an interference event will be valid for

at least two hours after. While the data bits themselves are not of interest, bit transitions must be accounted for in phase estimation.

Tracking GPS signals through wideband RFI requires coherent integration times (T_{coh}) longer than the duration of a GPS navigation data bit (20 ms). However, using larger values of T_{coh} means integrating I (in-phase) and Q (quadrature) samples across data bit transitions, effectively averaging them out over time. Potential PLL-based approaches to extend averaging time, such as use of noncoherent memory discriminators [2] or real-time bit estimation [3], introduce biases in the discriminator output, which causes errors in reconstructed carrier Doppler, ultimately leading to cycle slips. A more general problem using PLLs for carrier tracking is that they do not make optimal use of the available information in the GPS signal. This is an especially undesirable characteristic when the signal is already degraded by RFI.

Kalman filter implementations are far more flexible than PLLs [4]. They have been used to track phase through ionospheric scintillation in [5] [6] with $T_{coh} < 20$ ms and to track weak GPS signals with $T_{coh} > 20$ ms in [7] by augmenting with Bayesian bit estimation. Kalman filter carrier phase estimation with $T_{coh} > 20$ ms is a hybrid estimation problem, requiring simultaneous estimation of the discrete navigation data bits and the continuous carrier phase.

In this paper, we develop a new, computationally efficient phase estimator based the Interacting Multiple Model (IMM) algorithm to allow robust carrier phase estimation tracking through sustained RFI. In Section II, the IMM algorithm is explained and the component Kalman filters are set up. Section III derives a dynamic model for clock phase dynamics. Section IV describes the experimental scenario and setup. Section V provides and experimental validation of the IMM filter under normal conditions (no interference). Section VI optimizes the design of a typical PLL for interference robustness and provides experimental results under interference. Section VII shows the IMM filter experimental results under interference.

II. KALMAN FILTER AND IMM ALGORITHM

While typical PLLs only have fixed structure with predefined loop filters, Kalman filters have internal adaptability to

rely more heavily on either measurements or phase dynamics depending on the noise levels. Extended coherent averaging times are needed to track through interference. If there is no external information about the navigation data bits, the maximum coherent integration time is 20 ms, which is the duration of one navigation data bit. However, if possible, longer coherent integration times can help average out noise tremendously, resulting in much cleaner I and Q measurements.

In SDR architectures, carrier phase and code phase tracking loops start with the carrier frequency obtained from the acquisition process. Mixing the raw received signal with local sine and cosine waves at the acquired carrier frequency will produce I and Q measurements. Moving forward, the carrier tracking loop will update the local carrier frequency using I and Q measurements averaged over the each subsequent coherent integration window. Figure 1 shows the carrier phase tracking architecture in SDR.

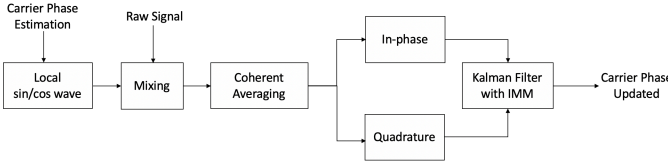


Fig. 1. Carrier phase tracking in SDR

Both the carrier phase and code phase tracking loops rely on the determination of carrier frequency which means the quality of I and Q measurements is extremely important. The interference event contributes additive white Gaussian noise (AWGN) directly into I and Q measurements. For typical PLL operation, using a simple phase discriminator, these noisy measurements can easily cause phase errors exceeding the pull-in limit of phase discriminator, usually leading to cycle slips and eventual loss of lock.

The shortcomings of a traditional PLL can be overcome using a Kalman filter to estimate phase directly. The goal of any carrier phase tracking loop is to produce best phase estimate under noisy conditions. The Kalman filter does precisely this given that the noise is white, which is the case in wideband interference. In our interference scenario, the receiver is running normally when hit by an RFI event, so Kalman filter estimate error is small at the start.

A. Dynamic model

The clock phase noise can be modeled using a 2^{nd} order system. The details of the model will be discussed in Section III.

$$\begin{bmatrix} \dot{\phi}_{clk} \\ \phi_{clk} \end{bmatrix}_{k+1} = \Phi \begin{bmatrix} \dot{\phi}_{clk} \\ \phi_{clk} \end{bmatrix}_k + w_k \quad (1)$$

where k is a time index defining the current coherent average interval.

Over one coherent averaging interval, the total phase change is $\Delta\phi_{tot} = \Delta\phi_{sm} + \phi_{clk}$, where $\Delta\phi_{sm}$ is the phase change

due to the movement of the satellite relative to the receiver. For our current development, we assume a static receiver – e.g., a GBAS reference receiver – so that $\Delta\phi_{sm}$ is the result of satellite motion only, which is known using the broadcast ephemeris. In the future work for moving users, the relative motion between satellite and receiver can be accommodated using inertial sensors.

B. Measurement model

The measurement model can be written as

$$I_k = d_k A_k \cos(\Delta\phi_{tot,k}) + v_{i,k} \quad (2)$$

$$Q_k = d_k A_k \sin(\Delta\phi_{tot,k}) + v_{q,k} \quad (3)$$

where d is the navigation data bit, A is the signal amplitude, and v_i and v_q are i.i.d. $\sim N(0, V)$, where $V = I\sigma_v^2$ and is related to the carrier-to-noise ratio as follows:

$$C/N_0 = 10 \frac{C/N_0(\text{dBHz})}{10} \quad (4)$$

$$\sigma_v = \frac{1}{\sqrt{0.04 C/N_0}} \quad (5)$$

C. IMM algorithm

The IMM is a multiple hypothesis estimation algorithm. It assumes a system obeys one of a finite number of models at a time [8]. It is composed of the five steps shown in Figure 2. Starting with prior probabilities of each model being correct, parallel Kalman updates are executed for each, and the mode likelihood functions are evaluated based on the measurements. Then post measurement mode probabilities are determined, and the results from all of the modes are weighted and combined to produce the output state vector estimate and its error covariance matrix.

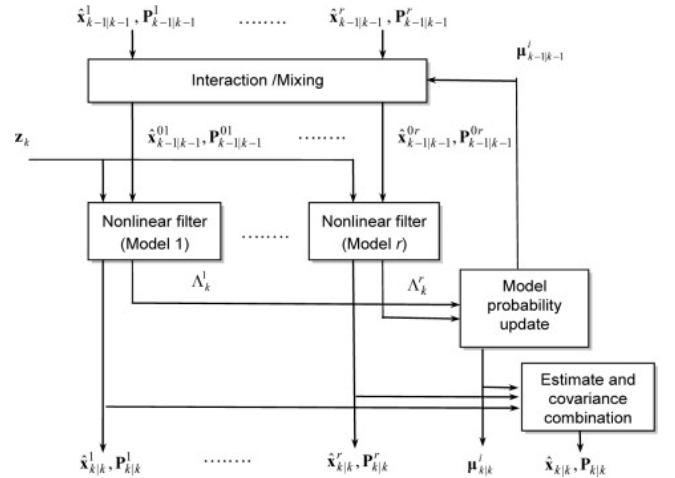


Fig. 2. IMM algorithm

In our IMM application, as shown in Figure 3, two modes run in parallel, corresponding to the two navigation data bits values, 1 and -1 . The mode (bit) transition probabilities are $\frac{1}{2}$ and $\frac{1}{2}$, which means the data bits are sequentially independent

of each other. However, the data bits in reality are not totally random. The knowledge of some navigation data bits can also be utilized by the IMM, as we have shown in our prior work [9]. We assume no such knowledge here.

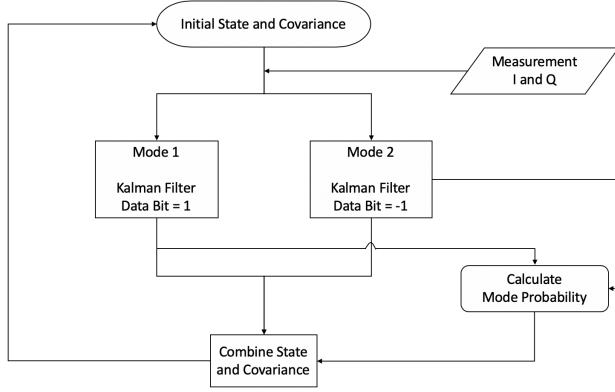


Fig. 3. IMM algorithm in our case

III. CLOCK DYNAMIC MODEL

We use separate Rubidium atomic oscillators (SpecrtaTime LPRFS) in our experimental work for the receiver and GPS signal simulator. The random fluctuation in phase, corresponding to jitter in time domain, is described by the clock's phase noise power spectral density (PSD), which is modeled as:

$$S(f) = h_2 f^0 + h_1 f^{-1} + h_0 f^{-2} + h_{-1} f^{-3} + h_{-2} f^{-4} \quad (6)$$

Unfortunately, the clock specifications did not cover the phase noise PSD in lower frequency ranges needed for our purpose. So we need to derive a set of h coefficients from Allan variance data.

A. Full Frequency Range Plot

The Allan variance plot shown as the blue curve in Figure 4 measures the short term stability of the clock. The slopes of the blue curve can be approximately matched to the terms in Equation 6 using three asymptotes from h_1, h_0 and h_{-1} . Using the relations shown in Figure 5 from [10], the following coefficients are selected: $h_2 = 0$, $h_1 = 1.0 \times 10^{-22}$, $h_0 = 3.4 \times 10^{-23}$, $h_{-1} = 4.6 \times 10^{-27}$, $h_{-2} = 0$.

B. State Space Realization

To implement clock dynamics in the IMM's Kalman filters, we write the transfer function in discrete state space form.

$$\begin{bmatrix} \phi \\ \dot{\phi} \end{bmatrix}_{k+1} = \begin{bmatrix} 1 & T_s \\ 0 & 1 \end{bmatrix} \begin{bmatrix} \phi \\ \dot{\phi} \end{bmatrix}_k + w_k \quad (7)$$

where the covariance matrix for w_k is

$$W = \begin{bmatrix} S_f T_s + \frac{S_g T_s^3}{3} & \frac{S_g T_s^2}{2} \\ \frac{S_g T_s^2}{2} & S_g T_s \end{bmatrix} \quad (8)$$

and $S_f = 2 \times 10^{-22}$, $S_g = 6.28 \times 10^{-31}$

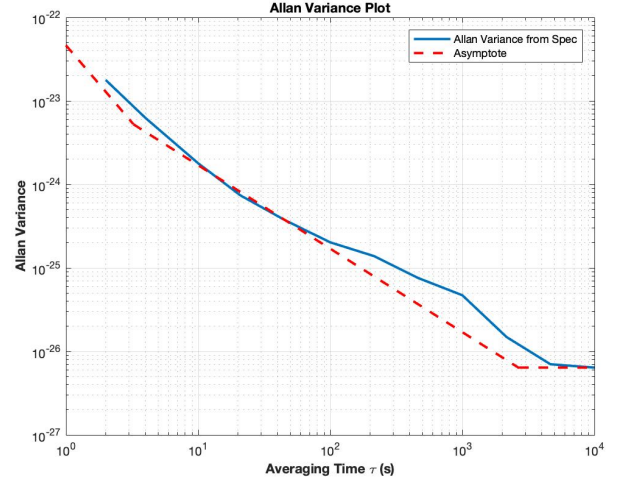


Fig. 4. Allan variance asymptotes

Description of noise process	$S_y(f) =$	$S_\phi(f) =$	$\sigma_y^2(\tau) =$
Random walk FM	$h_{-2} f^{-2}$	$h_{-2} \nu^2 f^{-4}$	$A h_{-2} \tau^1$
Flicker FM	$h_{-1} f^{-1}$	$h_{-1} \nu^2 f^{-3}$	$B h_{-1} \tau^0$
White FM	$h_0 f^0$	$h_0 \nu^2 f^{-2}$	$C h_0 \tau^{-1}$
Flicker PM	$h_1 f^1$	$h_1 \nu^2 f^{-1}$	$D h_1 \tau^{-2}$
White PM	$h_2 f^2$	$h_2 \nu^2 f^0$	$E h_2 \tau^{-2}$

$$A = \frac{2\pi^2}{3} \quad B = 2 \ln 2 \quad C = 1/2$$

$$D = \frac{1.038 + 3 \ln(2\pi f_h \tau)}{4\pi^2} \quad E = \frac{3 f_h}{4\pi^2}$$

Fig. 5. Allan variance calculation [10]

IV. EXPERIMENTAL SCENARIO AND SETUP

A. Experimental Scenario

In the interference scenario, the GPS receiver is operating under normal signal conditions prior to onset of the RFI event, so that the current ephemeris has already been decoded and will be valid for at least another two hours. The experiment covers a static GPS reference receiver over a 4 minute period with 4 satellites (PRN 7, 11, 28, 30) on a specific day. The ephemeris file over that period is provided to software defined receiver (SDR). High elevation satellites are used in this test to avoid other potential carrier phase estimation errors. The onset of the RFI event is 2 minutes after start so that the receiver has time to locked on to the nominal signals. The interference event is implemented by dropping C/N_0 from 45 dBHz (which was the nominal signal strength for all 4 satellites) as follows: no drop for PRN 30, 10 dBHz drop for PRN 7, 20 dBHz drop for PRN 11, and 30 dBHz drop for PRN 28.

B. Experimental Setup

GPS RF signals are generated using a Spectracom GSG-6 GNSS simulator. A USRP N200 is used as the front end

and, as noted earlier, two LPRFS Rubidium clocks are used as references for satellite and receiver. The IMM algorithm is implemented in a software defined receiver (SDR). Figure 6 shows the overview of the experimental setup.

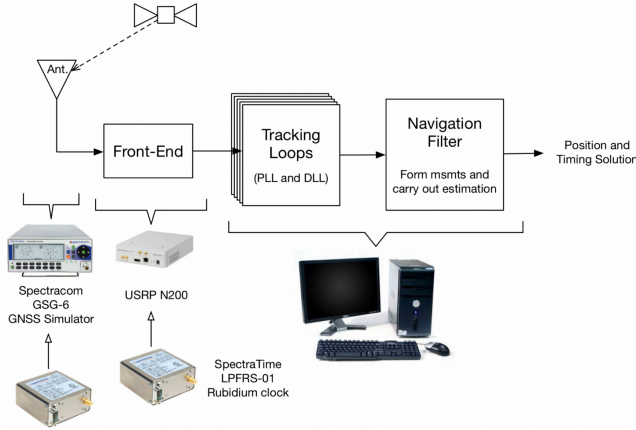


Fig. 6. Experimental setup

V. VALIDATION OF IMM FILTER

When no interference is present, the IMM filter is expected to have essentially the same “tracking” ability as a PLL. In this case, the PLL should provide a good reference for comparison. PRN 30 was free of interference over the entire 4-minute period, so it was used to test the IMM filter under nominal signal conditions. To do this we ran the PLL and IMM in parallel for PRN 30 and compared the reconstructed clock frequency output from both. If the reconstructed clock frequency is same from both, the total reconstructed carrier frequency will also be the same, because the remainder is due only to Doppler, which is also the same for both. As noted in section IV-A the ephemeris file is available, so the Doppler feed into PLL and IMM is the same.

Figure 7 shows the details of the processing algorithm. The PLL maintains carrier frequency and phase lock at all

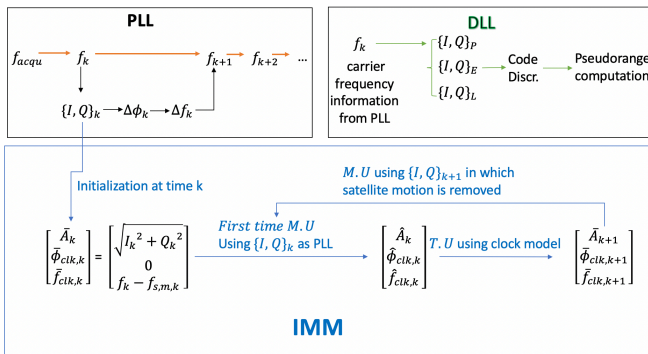


Fig. 7. IMM filter

times in this interference-free case, so the IMM can start at any time by taking the initial knowledge of the state vector

from the PLL. After that, the IMM runs independently in parallel to the PLL. The measurement and dynamic model are shown in section II-B and II-A. The DLL needs the current carrier frequency to operate, which typically comes from the PLL. However, after we validate the IMM filter, we can draw the carrier frequency from the IMM. In this test, typical parameters are initially used in PLL: 3 rd order loop filter, 15 Hz noise bandwidth, 1 ms coherent averaging time. The IMM filter starts at 80 sec.

Figure 8 and 9 show clock frequency results from PLL and IMM, respectively.

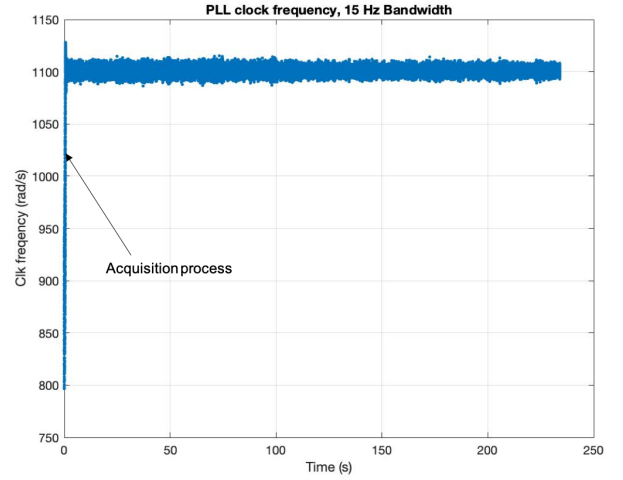


Fig. 8. PLL clock frequency, 15 Hz bandwidth

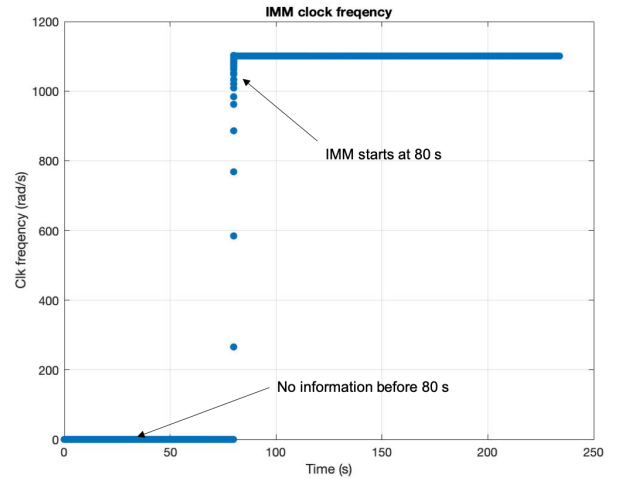


Fig. 9. IMM clock frequency

After the IMM filter starts at 80 sec, the main difference between these two figures is that PLL result has a large variance on clock frequency whereas IMM frequency result is nearly flat line centered at the same frequency. However, the comparison is not quite fair to the PLL because the IMM is designed to estimate only clock dynamic states, whereas

the nominal 15 Hz bandwidth of the PLL is designed to handle user motion. The equivalent noise bandwidth for IMM dynamic model in III is 0.16 Hz. This explains the superior performance of the IMM in these initial interference-free results. Therefore, we next passed the same raw data through the PLL again, but this time tightening the PLL bandwidth from 15 Hz to 1 Hz at 10 s. It was not feasible to tighten the bandwidth less than 1 Hz because of PLL stability issues. The result is shown in Figure 10. Figure 11 shows the difference between Figures 10 and 9. Figure 12 is a zoomed-in version of figure 11.

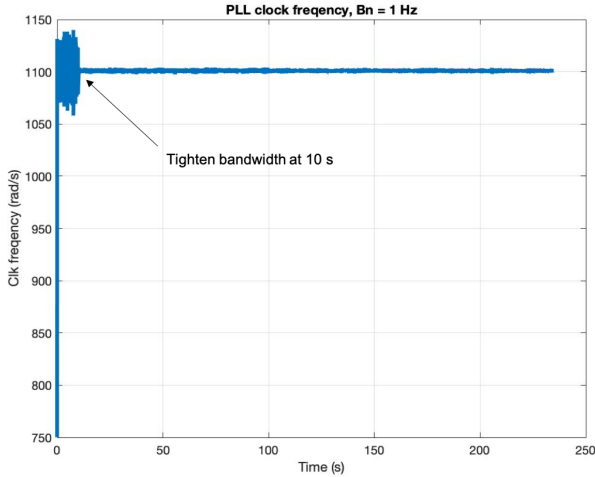


Fig. 10. PLL clock frequency, bandwidth tightened to 1 Hz

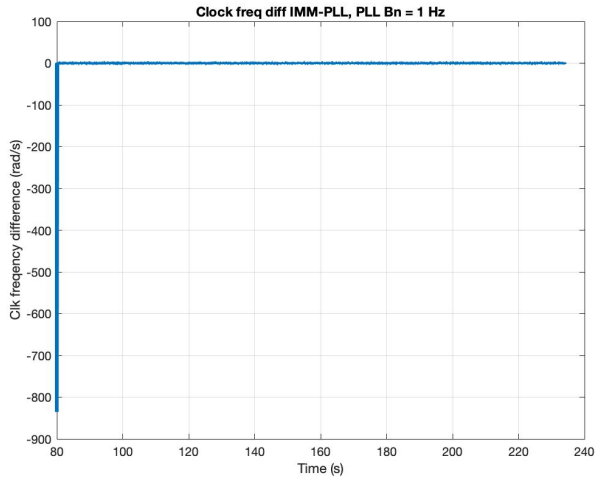


Fig. 11. Clock frequency difference, PLL bandwidth tightened to 1 Hz

As we tighten the PLL bandwidth down closer to IMM clock model bandwidth (0.16 Hz), the resulting clock frequency error variances become more similar. Figure 12 shows the difference between the IMM and new PLL results. Because the IMM and PLL produce the same clock frequency estimates, they will also provide the same carrier frequency

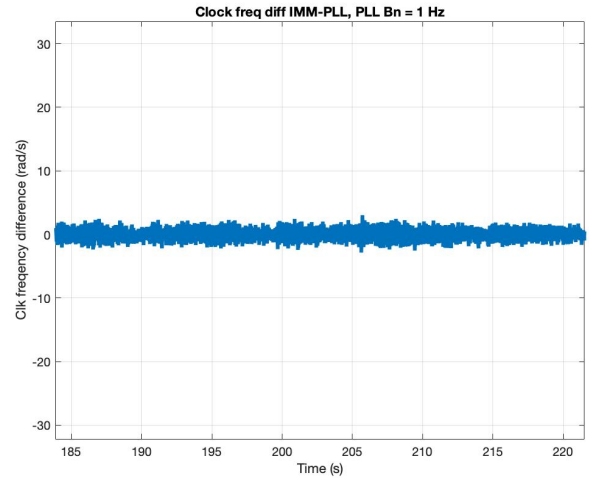


Fig. 12. Clock frequency difference zoomed-in

and phase results by adding the known Doppler the from ephemeris. Figures 13 and 14 show the reconstructed carrier phases from PLL and IMM, respectively. Figure 15 shows the difference of carrier phase outputs between the PLL and IMM. The variance of the error matches the expected tracking error variance of the PLL with 1 Hz for a 45 dBHz signal

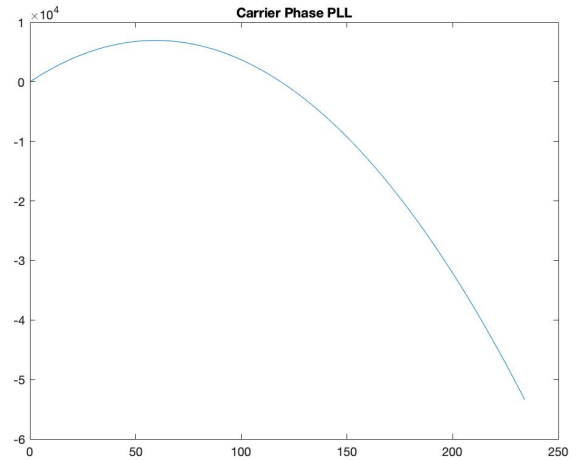


Fig. 13. PLL carrier phase, PLL bandwidth tightened to 1 Hz

VI. PLLS AND INTERFERENCE

Section V has so far validated that the performance of the IMM filter is as good as a PLL when there is no interference. The next step is to evaluate their relative performance during an interference event. To do a fair comparison with the IMM filter, we should make sure the PLL is doing its ‘best’ in interference case. There are two typical methods for PLL to handle noise, tightening the bandwidth and extending coherent averaging time.

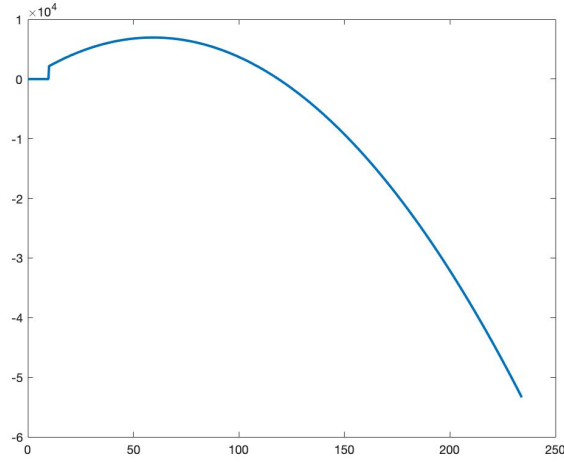


Fig. 14. IMM carrier phase estimation

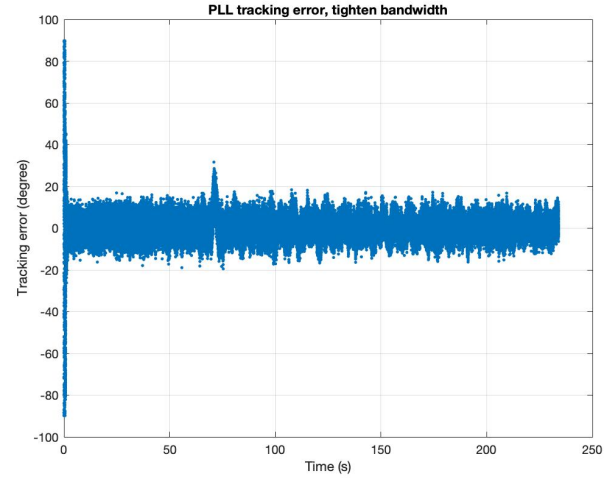


Fig. 16. Dynamic pattern when tighten bandwidth

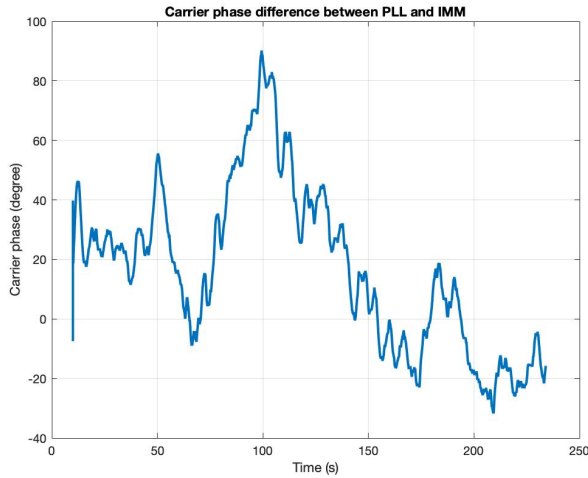


Fig. 15. Carrier phase difference

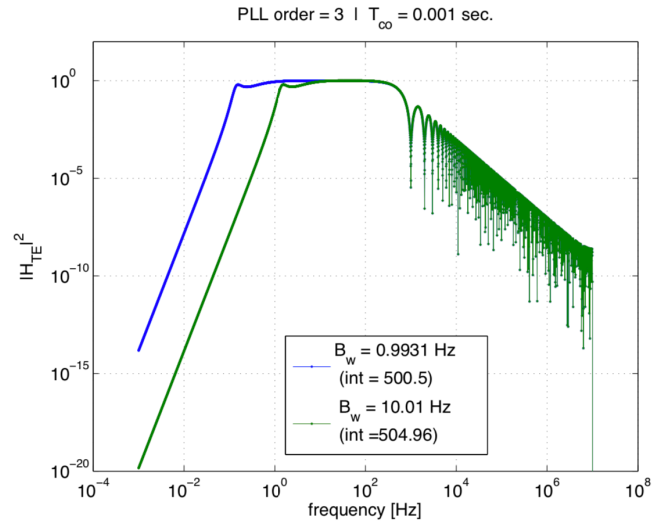


Fig. 17. Tracking error transfer functions for different PLL bandwidths

A. Tightening PLL Bandwidth

Our observations of preliminary experimental results showed that when coherent averaging times are increased rapid tightening of PLL bandwidth after acquisition can cause the PLL to become unstable. Thus, a smooth polynomial function, equation 9, was used to tighten the bandwidth B_n from 15 to 1 Hz in first 70 sec, and then keep it at 1 Hz for the rest of time.

$$B_n = 3e^{-19t^4} - 1.3e^{-13t^3} + 1.5e^{-8t^2} - 0.0007t + 15.15 \quad (9)$$

where t is the elapsed time. An example of the tracking error is shown Figure 16:

As Figure 16 shows, when we gradually tighten the bandwidth, signal content at lower frequencies (sinusoidal patterns) becomes more prominent. This result is consistent with analytical results in [3] as shown in Figure 17. When the bandwidth

is reduced, the first break frequency frequency of tracking error transfer function moves to the left (toward the low frequency direction), from the green line to blue line in Figure 17. Therefore, more low frequency content is allowed to pass through. This explanation was verified by taking the Fourier Transform of the data in Figure 16. The result in Figure 18 shows that the first break frequency matches the prediction in Figure 17.

B. Extending Coherent Averaging Time

Without an external source the navigation data bits, the coherent averaging time can be extended to up to a maximum of $T_{co} = 20$ ms.

Figure 19 shows example tracking error results where the coherent averaging time is increased from 1 ms to 20 ms at an elapsed time of 120 sec. As expected, with 20 ms co-

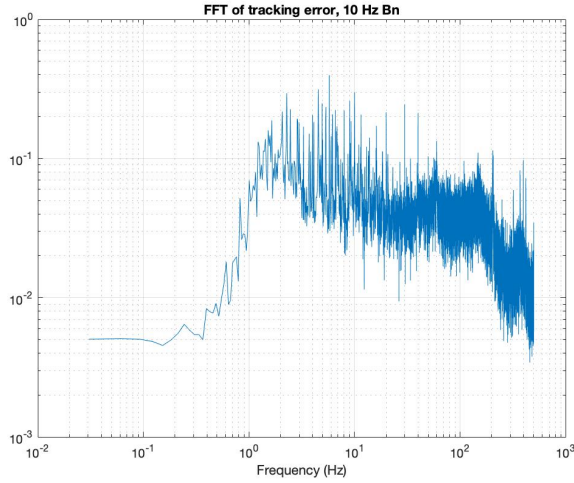


Fig. 18. Fourier Transform of data in Figure 16

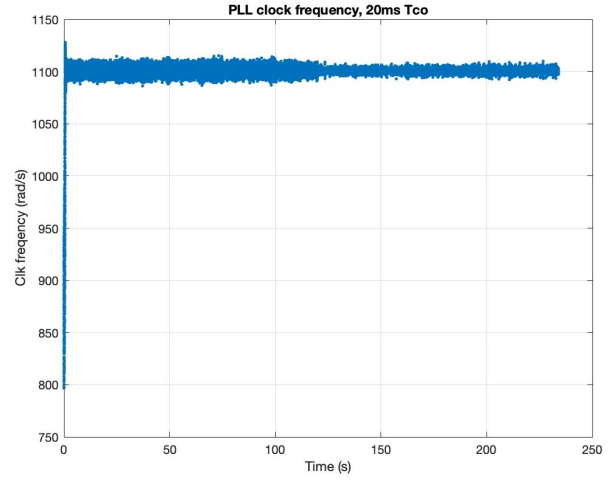


Fig. 20. PLL clock frequency, $T_{co} = 20$ ms

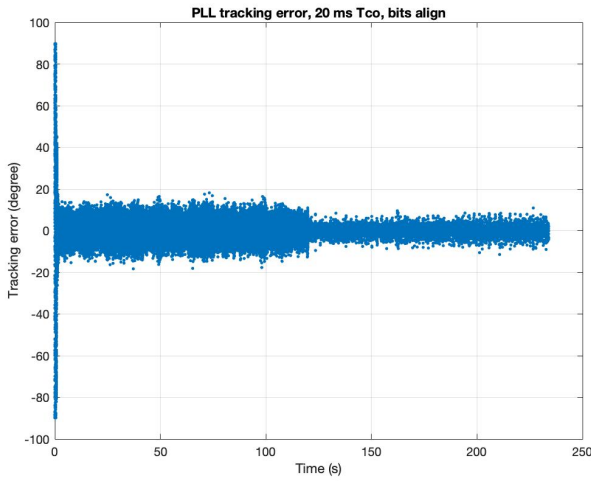


Fig. 19. Tracking error, T_{co} reduced from 1 ms to 20 ms at $t = 120$ sec

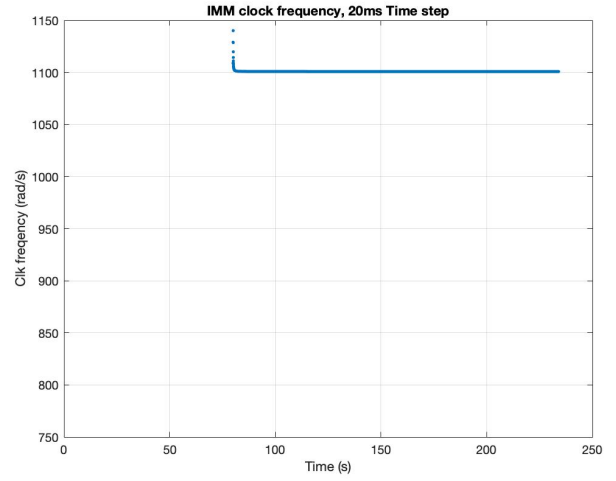


Fig. 21. IMM clock frequency, $T_{co} = 20$ ms

herent averaging, the variance of tracking error is significantly reduced.

VII. IMM FILTER PERFORMANCE IN INTERFERENCE

A. Validation of IMM with $T_s = T_{co} = 20$ ms

As was done in section V for $T_s = T_{co} = 20$ ms, we need to validate interference-free IMM performance at 20 ms. We gain use PRN 30 data and comparing clock frequency output results from the PLL and IMM. In this test, the PLL bandwidth is kept at 15 Hz throughout. Figures 20 and 21 show the PLL and IMM results, and Figure 22 is the difference between them.

As before, the PLL has a larger noise variance because it using large bandwidth as 15 Hz. But Figure 22 has a zero mean which means IMM filter result gives the same clock frequency estimation as the PLL.

B. Interference Case: 35 dBHz

We perform the same test as in VII-A for PRN 7 data, which has a 10 dBHz drop in C/N_0 at 110 s. The PLL is still using a 15 Hz bandwidth, but extended to 20 ms coherent averaging at 120 s to handle the increased noise. The IMM filter starts at 80 s with 20 ms time step.

From PLL phase tracking error results in Figure 23, it is clear that the phase tracking error variance increases after the interference hits (110 - 120 s) and then shrinks as we extend the coherent averaging time to 20 ms. Phase tracking error is always within PLL discriminator pull-in region because the 10 dB/Hz drop is not extreme, so the PLL is still able to maintain lock.

Figures 24 and 25 show the clock frequency results from the PLL and IMM, and Figure 26 shows the difference between them.

Again, the difference is mainly due the PLL's limited ability

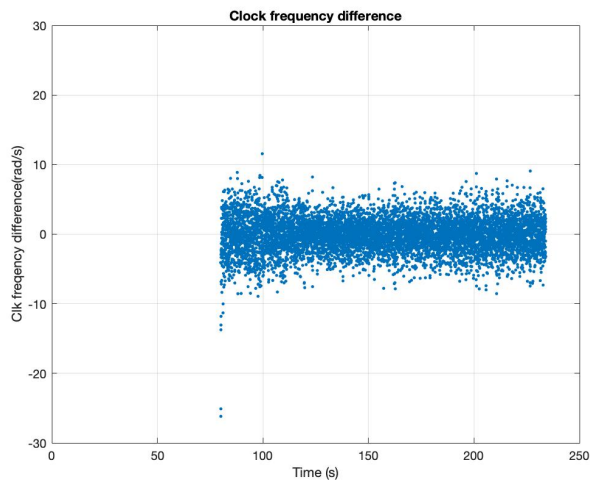


Fig. 22. Clock frequency difference, $T_{co} = 20$ ms

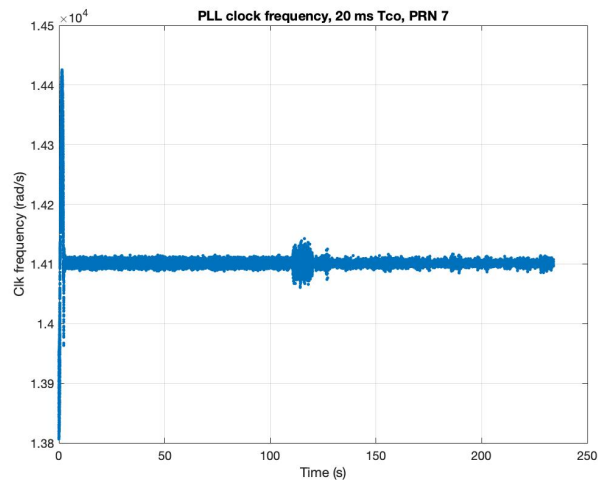


Fig. 24. PLL clock frequency, $T_{co} = 20$ ms, PRN 7

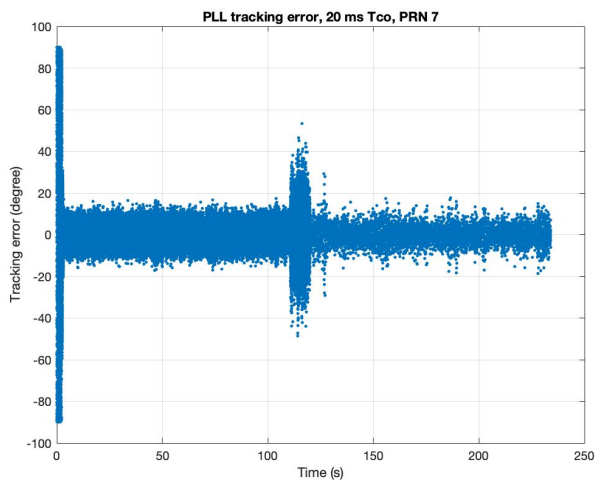


Fig. 23. PLL tracking error, 20 ms, PRN 7

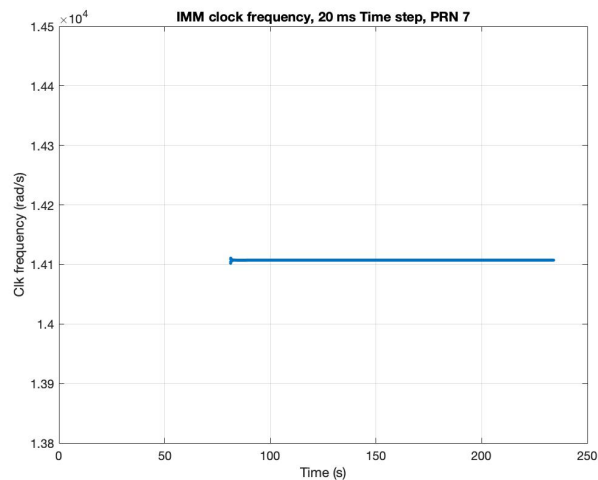


Fig. 25. IMM clock frequency, $T_{co} = 20$ ms, PRN 7

to handle noise. In contrast, IMM filter has a built in dynamic model and ability to adapt to modify (increase) input I and Q measurement error variances when C/N_0 is reduced. The following section ?? will provide stronger evidence for this conclusion. We note that, for the time being, we assume that existing C/N_0 estimators are sufficient for our purposes, but this needs will be verified in future work.

C. Interference Case: 15 dBHz

In this section, we test the IMM filter using PRN 28 data, which has a 30 dBHz C/N_0 drop. Although the PLL bandwidth has been tightened to 1 Hz and the coherent averaging time extended to 20 ms, it is still not possible for the PLL to track the signal at 15 dB/Hz C/N_0 , simply because the noise is huge. Figure 27 shows the tracking error plot for the PLL. Total loss of lock occurs when the interference hits because the PLL's discriminator can no longer extract any information from the I and Q measurements.

The PLL's clock frequency results are also very poor as shown in Figure 28. Beginning at 110 sec, the frequency reconstruction from the PLL drifts away.

However, the IMM filter is still able to provide accurate clock frequency estimation. Figure 29 shows the IMM clock frequency estimation result, and Figure 30 shows the final carrier phase reconstruction result from the IMM.

The results show that the IMM filter is able to provide good carrier phase output even through an interference event with $C/N_0 = 15$ dB/Hz, while the PLL immediately loses lock even when coherent averaging time and bandwidths are, respectively, set their maximum and minimum values.

VIII. CONCLUSION

In this paper, we develop an IMM carrier phase estimation algorithm to allow GPS receivers to maintain continuous signal tracking through wideband radio frequency interference events.

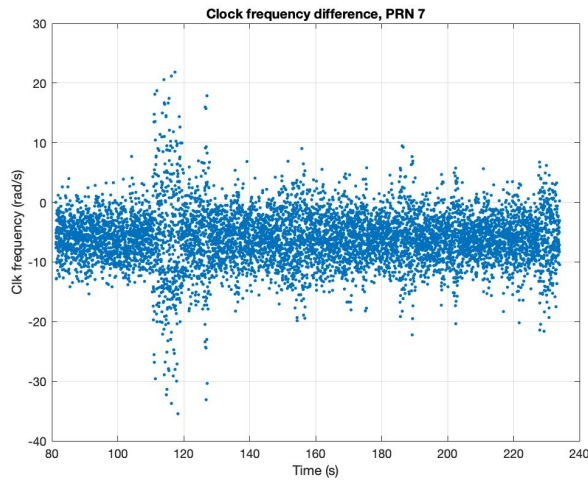


Fig. 26. Clock frequency difference, $T_{co} = 20$, PRN 7

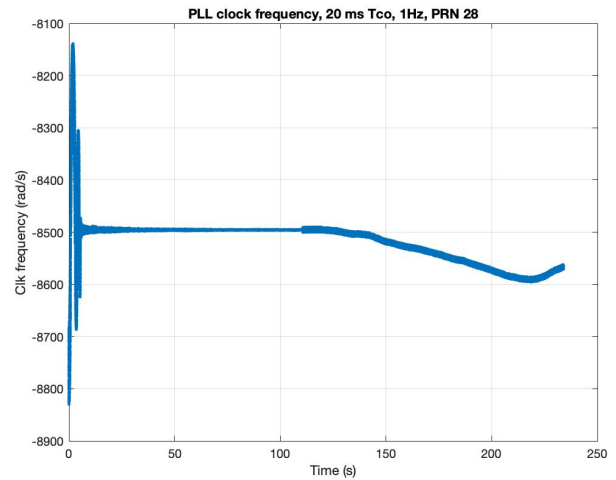


Fig. 28. PLL clock frequency, PRN 28

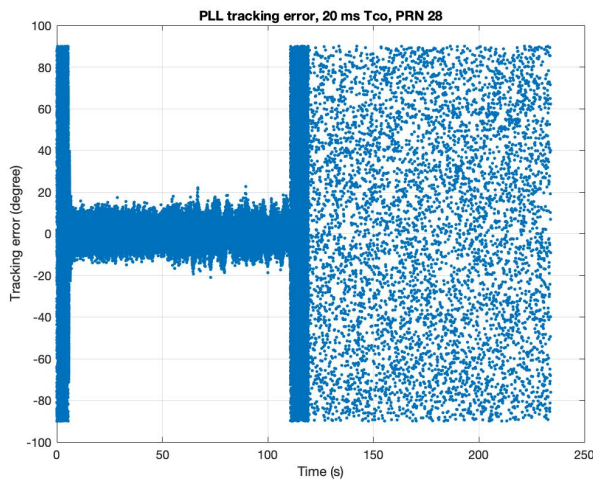


Fig. 27. PLL tracking error, 20 ms, 1Hz, PRN 28

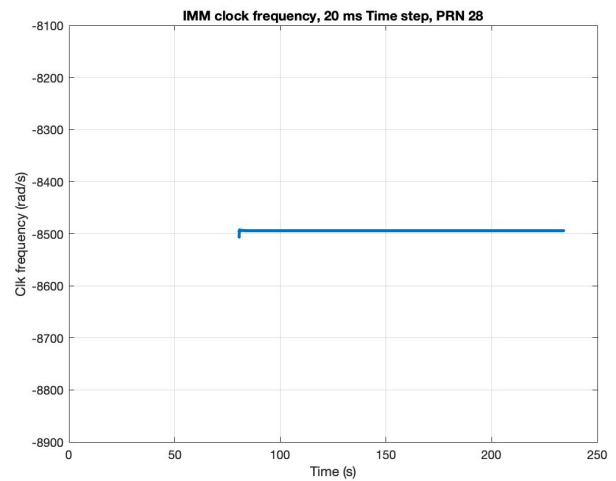


Fig. 29. IMM clock frequency, PRN 28

The IMM algorithm and its component Kalman filters were shown to work well for carrier phase tracking in both simulations in our previous work [11] and in experiments, in this paper. The experimental results show that the IMM is able to track as well as (or slightly better than) a traditional PLL under normal signal levels (no interference). They also show that during interference events down $C/N_0 = 15$ dB/Hz the IMM filter is able to provide correct carrier phase estimation while the PLL can no longer maintain lock.

In future work, navigation data bit structure information will be used. Adaptive noise variance estimation will also be added to the IMM. The transition matrix between each noise levels needs to be modeled in this case. The algorithm will also be applied to moving receivers with Doppler aiding from inertial sensors.

ACKNOWLEDGMENT

We would like to thank our sponsors at the Federal Aviation Administration (FAA) for supporting this research. The views and opinions expressed in this paper are those of the authors and do not necessarily reflect those of any other organization or person.

REFERENCES

- [1] Pullen, S., and Gao, G. *GNSS Jamming in the Name of Privacy: Potential Threat to GPS Aviation*; Inside GNSS Magazine: Vol. 7 No. 2, March/April 2012.
- [2] Borio, Daniele, and Gard Lachapelle. *A non-coherent architecture for GNSS digital tracking loops*; annals of telecommunications-Annales des telecommunications 64.9-10 (2009): 601.
- [3] Stevanovic, S and Pervan, B. *Coasting Through Wideband Interference Events using Robust Carrier Phase Tracking*; In Proceedings of the 30th International Technical Meeting of the Satellite Division of the Institute of Navigation (ION GNSS+ 2017), 2017.

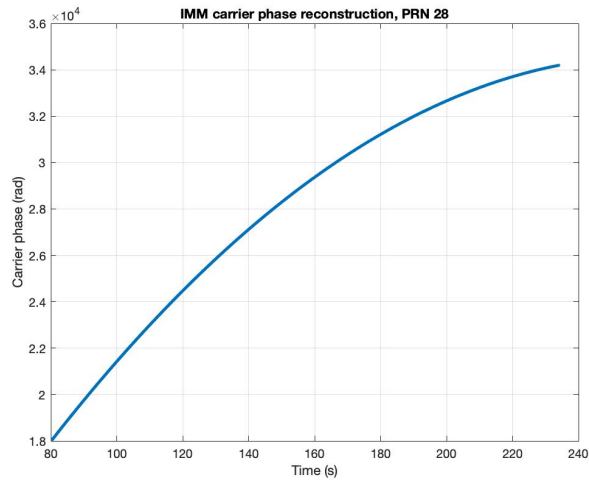


Fig. 30. IMM carrier phase reconstruction, PRN 28

- [4] Vila-Valls, J. and P. Closas and M. Navarro and C. Fernandez-Prades. *Are PLLs dead? A tutorial on Kalman filter-based techniques for digital carrier synchronization*; IEEE Aerospace and Electronic Systems Magazine, Volume 32, Issue 7, 2017.
- [5] Vila-Valls, J. and P. Closas, and C. Fernandez-Prades. *Advanced KF-based methods for GNSS carrier tracking and ionospheric scintillation mitigation*; Aerospace Conference, 2015 IEEE. IEEE, 2015.
- [6] Humphreys, Todd E., Mark L. Psiaki, and Paul M. Kintner. *Modeling the effects of ionospheric scintillation on GPS carrier phase tracking*; IEEE Transactions on Aerospace and Electronic Systems 46.4 (2010): 1624-1637.
- [7] Psiaki, Mark L. *Extended Kalman filter methods for tracking weak GPS signals*; Proceedings of the 2002 ION GPS Conf., Portland, Oregon. 2002.
- [8] Bar-Shalom Yaakov and Li, X Rong and Kirubarajan, Thiagalingam *Estimation with applications to tracking and navigation: theory algorithms and software*; John Wiley & Sons, 2004
- [9] Zhao, Wengxiang, Pervan, Boris *IMM Methods for Carrier Phase Tracking and Navigation Data Bits Estimation Through Interference*; Proceedings of the 2019 International Technical Meeting of The Institute of Navigation, Reston, Virginia, January 2019, pp. 248-256.
- [10] *IEEE frequency and time standard*; pg.27
- [11] Zhao, Wengxiang, Pervan, Boris *Experimental Validation of IMM Algorithm for Carrier Phase Tracking Through Interference*; Proceedings of the 2020 International Technical Meeting of The Institute of Navigation, San Diego, California, January 2020, pp. 315-319.